Doppler-Resistant Orthogonal Chirp Division Multiplexing With Multiplex Resampling for Mobile Underwater Acoustic Communication

PEIBIN ZHU[1], GUANGSONG YANG[1], WEN CHEN[1], XIAOMEI XU[2], AND YOUGAN CHEN[2], (Senior Member, IEEE)

[1]School of Ocean Information Engineering, Jimei University, Xiamen 361021, China
[2]College of Ocean and Earth Sciences, Xiamen University, Xiamen 361005, China

Corresponding author: Peibin Zhu (peibin.dzhu@jmu.dedu.dcn)

ABSTRACT Mobile underwater acoustic communication technology has been widely employed in marine measurement and offshore engineering. The irregular relative motion between the transmitter and receiver causes time-varying Doppler shifts, which can cause severe inter-carrier interference (ICI) and thus affect the performance of orthogonal chirp division multiplexing (OCDM) communication. Conventional techniques such as resampling and residual carrier frequency offset can only handle constant Doppler frequency shift. In this paper, we propose a new method for handling time-varying Doppler shifts by adding multiplex resampling to OCDM communications. This method extends the resampling range based on the measured Doppler standard deviation and thus reduces the bit error rate (BER) in mobile underwater acoustic communications. The application of the variable number of branches in multiplex resampling reduces the computational complexity and saves the computational cost by approximately 30% compared with the fixed number of branches. We detail the implementation and parameter selection of the Doppler-resistant OCDM in mobile underwater acoustic communication, and compare the performance of multiplex resampling and single resampling by simulation and actual measurement in Qiandao Lake. The BER and frame error ratio (FER) results verify the feasibility of the proposed method and the superiority of its anti-time-varying Doppler shifts performance.

INDEX TERMS Time-varying Doppler shifts, orthogonal chirp division multiplexing, multiplex resampling, underwater acoustic communication.

I. INTRODUCTION

Presently, underwater acoustic communication (UWAC) technology has become the core technology for underwater engineering projects. As autonomous underwater vehicles (AUVs) and remotely operated underwater vehicles (ROVs) are widely employed in marine measurement and offshore engineering, the demand for mobile UWAC is increasing [1]. In AUVs and ROVs, mobile UWAC is crucial for the reliable transmission of control commands and data such as images or videos. In previous work, we adopted

The associate editor coordinating the review of this manuscript and approving it for publication was Fang Yang.

orthogonal chirp division multiplexing (OCDM) as the multi-carrier modulation method for anti-multipath UWAC [2].

AUVs and ROVs require reliable mobile UWAC. From a physical layer design perspective, the shallow water acoustic channels (active areas for AUVs and ROVs) are challenging environments characterized by a severe spread in time and frequency [3], [4]. Although OCDM is robust against multipath interference, it is also susceptible to Doppler as other multi-carrier communications such as orthogonal frequency division multiplexing (OFDM) [5]. Because the signal bandwidth is much larger than the inverse delay spread and because of the low speed of sound propagation in water (approximately 1500 m/s) [6], the Doppler shift has a significant impact on the broadband modulation of OCDM and
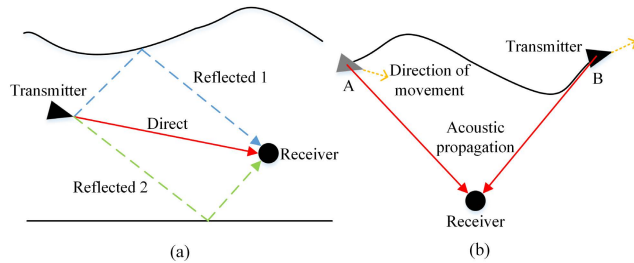
FIGURE 1. Classification of the non-uniform Doppler shifts. (a) Doppler spread and (b) time-varying Doppler shifts.

will cause inter-carrier interference (ICI). Therefore, Doppler compensation is essential for multi-carrier communication on mobile platforms such as AUVs and ROVs [7], [8].

If the Doppler shift is constant and known, i.de., there is a constant relative movement between the transmitter and receiver, Doppler compensation can be performed flawlessly by resampling and residual carrier frequency offset (CFO) correction techniques [9], [10]. However, in the practical UWAC system, the non-uniform Doppler shifts in a data frame must be considered. The non-uniform Doppler shifts can be classified into time-varying Doppler shifts and Doppler spread, as shown in Fig. 1.

Doppler spread is caused by the variability of underwater acoustic propagation, which occurs when each sound propagation path has a separate Doppler scale factor. As shown in Fig. 1(a), the transmitter moves in the same direction as the direct wave, while the remainder of the reflected waves travel in different directions, thus causing a slightly different Doppler shift between the direct and reflected waves. Underwater acoustic propagation produces many reflected waves, which in conjunction with different Doppler shifts are received and measured at the receiver to form the Doppler spread. Some recent papers have proposed anti-Doppler spread methods, such as Bayesian resampling [11], multiple resampling [12], frequency domain oversampling [13], and Doppler-resilient orthogonal signal-division multiplexing based on basic expansion model (BEM) [14]. However, the method of anti-Doppler spread is not the focus of this paper.

The time-varying Doppler shifts caused by the irregular relative motion between two transceivers have a great impact on mobile underwater acoustic communication. As shown in Fig. 1(b), when the transmitter moves along a curved trajectory, the Doppler shift should be positive at point A and negative at point B according to the relationship between underwater acoustic propagation and the velocity vector of the transmitter movement. Therefore, the resulting Doppler shift varies rapidly between positive and negative values. Due to the difficulty of modeling underwater acoustic propagation, few papers have proposed effective methods to solve the problem of time-varying Doppler shifts. The research in [15] has proposed linear multi-scale compensation by smoothing the estimated Doppler scale, which is suitable for the case where the Doppler shift linearly

changes. The authors utilize the inverse of ICI matrix by Jacobi iterative method to compensate Doppler effect in [16]. However, the computational complexity is too high to be practical. The research in [17] proposes the modified variable range resampling technique to handle the situation where the Doppler scaling factor changes slowly. In addition, [18] simplifies the Doppler compensation model by Taylor series expansion to reduce the amount of computation. None of the above methods can solve the problem of time-varying Doppler shifts. However, it can be seen that the resampling process is a critical part to alleviate nonuniform Doppler shifts. Therefore, it is necessary to propose a new method for time-varying Doppler shifts to improve the UWAC reliability of mobile platforms.

OCDM is a new multi-carrier modulation system designed for optical fiber communication. OCDM uses a set of orthogonal chirp signals for symbol modulation. Therefore, OCDM maximizes spectral efficiency while maintaining the robustness of chirp spread spectrum (CSS) technology [19]. Compared with the OFDM system, the OCDM system offers better anti-interference ability while maintaining the same spectral efficiency [5]. In previous work, we added a data pick-based rake receiver to the OCDM UWAC system for maintaining good anti-multipath performance in a shallow water environment, even at short guard intervals [2].

This paper proposes a new method for handling time-varying Doppler shifts by adding multiplex resampling to OCDM communications.

- We extend the resampling range based on the measured Doppler mean and standard deviation.
- Multiplex resampling modules are used to resample the OCDM data block. The optimal resampling ratio is selected by checking for errors and thus reduces the bit error rate (BER) in mobile underwater acoustic communications.
- We add a dynamic adjustment mechanism to the multiplex resampling receiver, which can control the number of branches of multiplex resampling frame by frame according to the statistics of the Doppler shift, thus reducing the amount of computation.

This paper is structured as follows: Section II describes the basic principles of OCDM and the multiplex resampling receiver. The channel models and the transmission scheme of the Doppler-resistant OCDM system are detailed in Section III. Section IV reports and discusses the simulation and experimental results in mobile UWAC. Section V summarizes this article.

II. PRINCIPLE OF DOPPLER-RESISTANT OCDM
A. OCDM BASICS
OCDM is based on Fresnel transform. Fresnel transform is an important transformation derived from classical optics [20], and its core basis is the chirp signal. We can synthesize a bank of N orthogonal and linear chirps as the core basis of the OCDM system, represented by $\psi_n(t)$,

which can be expressed as:

$$\psi_n(t) = e^{j\frac{\pi}{4}} e^{-j\pi \frac{N}{T^2}(t-n\frac{T}{N})^2}, \quad 0 \le t \le T \quad (1)$$

where n is the index of the chirp waveforms, N is the number of chirp waveforms, and T is the duration of chirp waveforms. The proposed OCDM achieves the maximum spectral efficiency for CSS in the sense of orthogonality. It can be easily proved in (2) that the set of chirp signals are mutually orthogonal:

$$\int_0^T \psi_m^*(t)\psi_k(t)dt$$
$$= \int_0^T e^{j\pi \frac{N}{T^2}(t-m\frac{T}{N})^2} e^{-j\pi \frac{N}{T^2}(t-k\frac{T}{N})^2} dt = \delta(m-k) \quad (2)$$

In a severe multipath underwater acoustic channel, the amplitude of the received waveform rapidly changes. Here, we choose QPSK as the modulation method. Denoting the kth symbol as $x(k)$ after QPSK mapping, the baseband time-domain OCDM signal $s(t)$ is then expressed as:

$$s(t) = \sum_{k=0}^{N-1} x(k)\psi_k(t), 0 \le t \le T \quad (3)$$

According to the orthogonality in (2), $x(m)$ can be easily extracted by the matched filter:

$$x'(m) = \int_0^T s(t)\psi_m^*(t)dt$$
$$= \sum_{k=0}^{N-1} x(k)\delta(m-k) = x(m) \quad (4)$$

According to (3) and (4), the multiplexing at the transmitter and demultiplexing at the receiver in the OCDM system are shown in Fig. 2.

OCDM can be realized in the digital domain by inverse discrete Fresnel transform (IDFnT). At the transmitter, the discrete time-domain OCDM signal $s(n)$ is obtained by sampling the analog signal in (3) as:

$$s(n) = F_\psi^{-1}\{x(k)\}$$
$$= \begin{cases} \sum_{k=0}^{N-1} x(k)\psi_k(n\frac{T}{N}) & N \equiv 0 (\mathrm{mod}2) \\ \sum_{k=0}^{N-1} x(k)\psi_k(n\frac{T}{N}+\frac{T}{2N}) & N \equiv 1 (\mathrm{mod}2) \end{cases}$$
$$= e^{j\frac{\pi}{4}} \sum_{k=0}^{N-1} x(k) \times \begin{cases} e^{-j\frac{\pi}{N}(n-k)^2} & N \equiv 0 (\mathrm{mod}2) \\ e^{-j\frac{\pi}{N}(n-k+\frac{1}{2})^2} & N \equiv 1 (\mathrm{mod}2) \end{cases}$$
$$(5)$$

In an actual OCDM UWAC system, N is usually selected as an even number to facilitate calculation. According to (5), OCDM modulation can be expressed as a compact matrix form, as follows:

$$\mathbf{s} = \mathbf{\Phi}^H \mathbf{x} \quad (6)$$
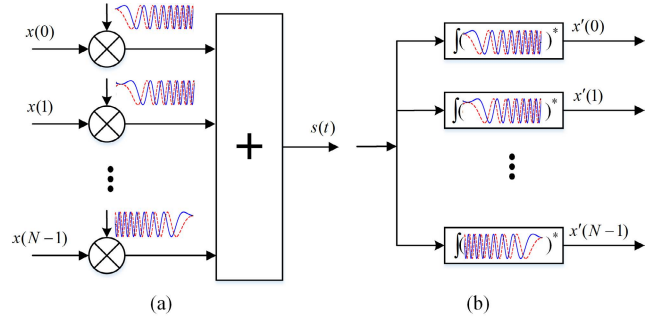

FIGURE 2. Schematic of the OCDM system (a) multiplexing and (b) demultiplexing a bank of N modulated orthogonal chirp waveforms.

where $\mathbf{s} = [s(0), s(1), \ldots, s(N-1)]^T$ is the discrete-time domain signal after OCDM modulation, $\mathbf{x} = [x(0), x(1), \ldots, x(N-1)]^T$ is the symbol vector after mapping, and $\mathbf{\Phi}$ is discrete Fresnel transform (DFnT) matrix. For the case where N is even, the matrix $\mathbf{\Phi}$ can be expressed as:

$$\{\mathbf{\Phi}\}_{n,k} = \frac{1}{\sqrt{N}} e^{-j\frac{\pi}{4}} e^{j\frac{\pi}{N}(n-k)^2} \quad (7)$$

Since the DFnT matrix is a unitary matrix, at the receiver, the transmitted symbol can be recovered by the inverse operation DFnT of (6), as follows:

$$\mathbf{x}' = \mathbf{\Phi}\mathbf{s} = \mathbf{x} \quad (8)$$

B. RESAMPLING AND FREQUENCY DOMAIN OVERSAMPLING

Since the speed of underwater acoustic propagation is much lower than that of electromagnetic waves, the Doppler effect has a significant impact on ICI-sensitive multi-carrier UWAC. The relative Doppler shift Δ is defined as the ratio of the relative velocity between the transmitter and receiver to the underwater sound propagation velocity. For a signal with a single frequency component f, the Doppler effect can be expressed by frequency scaling:

$$f' = f(1+\Delta) \quad (9)$$

For the wideband signal of UWAC, each frequency component has a different Doppler shift. The Doppler effect for broadband signals is generally modeled by the time scaling (expansion or compression) of the signal waveform [12]:

$$r(t) = s((1+\Delta)t) \quad (10)$$

In (10), $s(t)$ and $r(t)$ are the transmitted signal and received signal, respectively. $s[nT_s]$ can be obtained by discrete time sampling of the transmitted signal, where T_s is the sampling period, and the received signal $r[nT_s]$ can be expressed as:

$$r[nT_s] = s[(1+\Delta)nT_s] \quad (11)$$

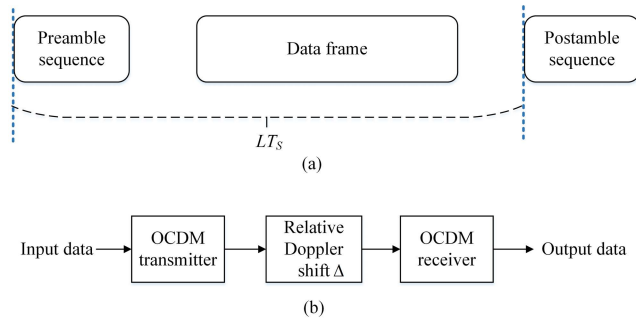According to (11), the resampling ratio should be $1/(1+\Delta)$, and the Doppler shift can be eliminated by the

FIGURE 3. (a) Frame format for Doppler estimation; (b) simple OCDM model with Doppler shift.

TABLE 1. OCDM system simulation parameters.

Symbol	Signification	Setting
B	Bandwidth for baseband signal	30 kHz
f_s	Sampling frequency	200 kHz
f_c	Center frequency	45 kHz
N	Number of subcarriers	1024
N_d	Number of data blocks per frame	10
T_{CP}	Cyclic prefix time	8.5 ms
T_G	Guard interval time after preamble sequence	128 ms
	Modulation	QPSK-OCDM
M	Constellation order	4
	FEC	Convolutional coding & Viterbi decoding
R_C	FEC rate	3/4
R_{CP}	Cyclic prefix ratio	1/4
	SNR	30 dB
α	Frequency domain oversampling factor	1 or 2

FIGURE 4. Tolerance for Doppler estimation errors. (a) EVM and (b) BER.

following equation:

$$r[\frac{1}{1+\Delta}nT_s] = s[nT_s] \tag{12}$$

Doppler estimation for resampling is usually performed by inserting a known sequence into the communication frame. As shown in Fig. 3(a), a standard method detects the arrival time difference between the preamble and the postamble [21]. Doppler shift can be measured by the change in signal length $(1 + \Delta)LT_s$, where LT_s is the time interval between the preamble and the postamble.

The simple OCDM model in Fig. 3(b) allows us to investigate the tolerance of Doppler estimation error. We add the relative Doppler shift to the OCDM transmit signal, and the channel model is a simple two-path model. The OCDM system simulation parameters are listed in Table 1.

The simulated error vector magnitude (EVM) and BER results are plotted in Fig. 4. The horizontal axis shows the Doppler shift that corresponds to the residual error of Doppler estimation. The results in Fig. 4(a) and 4(b) show that bit errors occur when the EVM exceeds 40%.
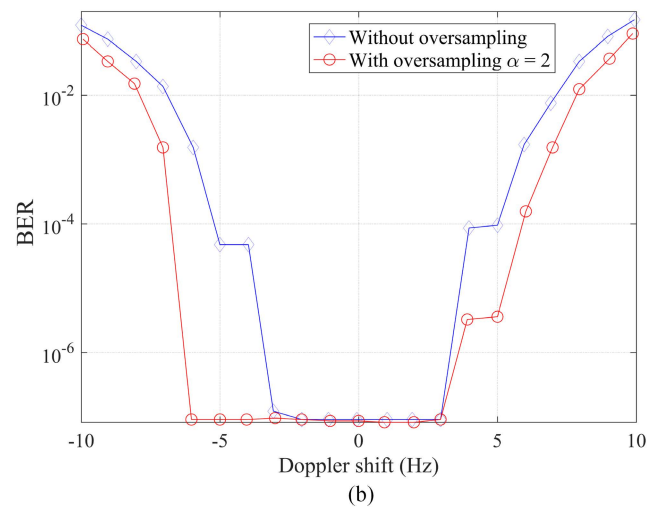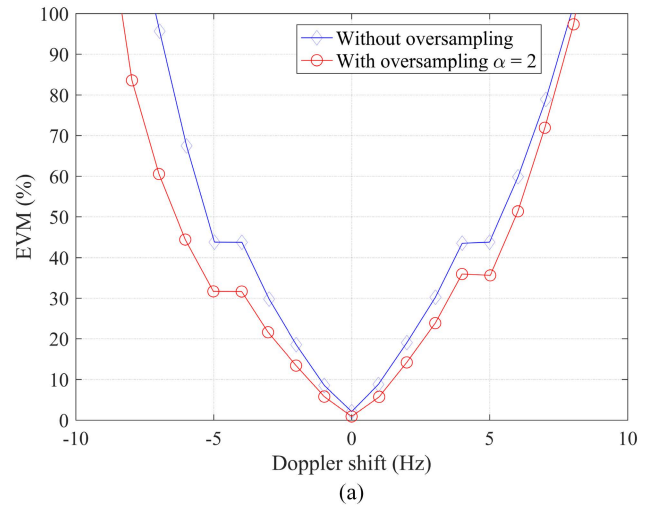
Since the center carrier frequency is 45 kHz, a Doppler shift of 4.5 Hz is equivalent to a relative Doppler shift of 1/10000. This result indicates that a maximum resolution of 1/10000 is required within the allowable resampling ratio error. The error tolerance can be extended by frequency domain oversampling [13], but the tolerance is still less than 5 Hz after frequency domain oversampling. Assuming a Doppler deviation of 10 Hz (measured in Section IV), frequency domain oversampling alone cannot cope with such large time-varying Doppler shifts.

C. MULTIPLEX RESAMPLING RECEIVER
To investigate the influence of time-varying Doppler shifts, we simulate the OCDM system performance by applying various Doppler shift patterns into OCDM data blocks. The time-varying Doppler shifts shown in Fig. 5 are explained by comparing the two Doppler shift models. The constant Doppler shift model refers to the direction of sound propagation, which is the same as the transmitter velocity vector, where the constant Doppler shift is assumed to be Δ_C. The time-varying Doppler shifts model refers to the
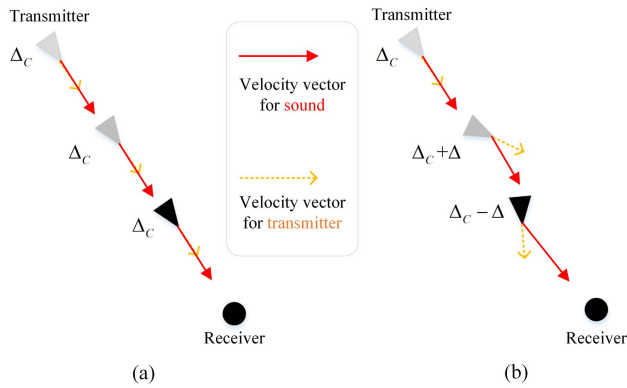
FIGURE 5. Doppler shift models. (a) Constant Doppler shift and (b) time-varying Doppler shifts.
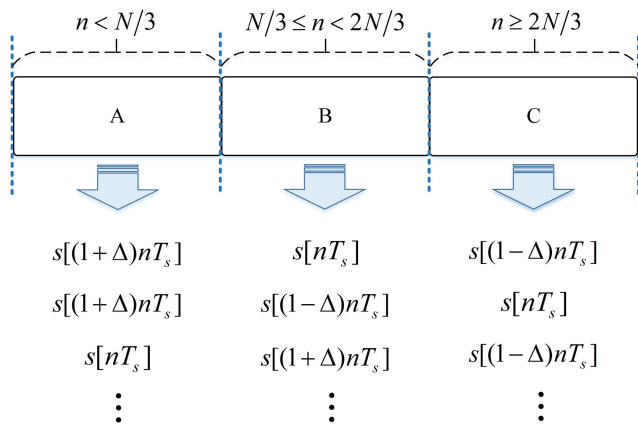

FIGURE 6. OCDM data block with a Doppler shift pattern.

FIGURE 7. OCDM model with doppler shift.

TABLE 2. EVM results for various doppler shift patterns and resampling ratios.

Doppler shift patterns			Resampling ratios				
A	**B**	**C**	$1/(1-\Delta)$	$1/(1-\Delta/2)$	1	$1/(1+\Delta/2)$	$1/(1+\Delta)$
1	Δ	0	$-\Delta$	76.9	36.1	36.3	90	128.8
2	Δ	$-\Delta$	0	131.8	83.1	35.1	32.6	80.3
3	0	Δ	$-\Delta$	137.5	160.8	47.4	29.9	60
4	0	$-\Delta$	Δ	154.3	122.3	68	57.2	103.1
5	$-\Delta$	Δ	0	197.2	149.1	119.6	62.1	29.9
6	$-\Delta$	0	Δ	188.8	163.6	71.4	21.8	32.2

movement direction of the transmitter, which continuously changes within the duration of an OCDM frame. The Doppler shift changes are Δ_C, $\Delta_C + \Delta$, and $\Delta_C - \Delta$ due to the relation between sound propagation and the transmitter velocity vectors.

Since the constant Doppler shift Δ_C can be eliminated by topical Doppler compensation techniques [9], [10], the cases where the Doppler shifts are 0, Δ, and $-\Delta$ can be considered by setting $\Delta_C = 0$. Fig. 6 illustrates an OCDM data block with a Doppler shift pattern. An OCDM data block of length N is divided into three sections A, B, and C. Various Doppler shift patterns are produced by shuffling the Doppler shifts into three sections so that all the shifts are allocated in a data frame. Although more complex Doppler shift patterns should be considered in practical UWAC, the simplified pattern is convenient for analysis and discussion, and the proposed multiplex resampling can cope with any unknown Doppler shift patterns. We construct multiple Doppler shift patterns (representing random motion at the transmitter) by randomly arranging the three Doppler shifts of 0, Δ, and $-\Delta$. Random positive and negative variations of the Doppler shift throughout the data frame can be observed in simulation, as will be shown in Section IV.
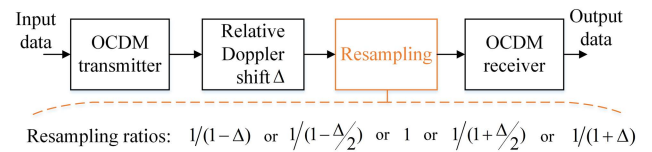
The resampling process is shown in Fig. 7, and each resampling ratio is evaluated as $1/(1-\Delta)$, $1/(1-\Delta/2)$, 1, $1/(1+\Delta/2)$, and $1/(1+\Delta)$. We assume that the variation range of the transmitter speed is ±1.2 km/h and that the maximum Doppler shift is $\Delta \cdot f_C = 10$ Hz, where $f_C = 45$ kHz denotes the center frequency of the OCDM system. The remainder of the simulation parameters are equivalent to those in Table 1, and the frequency domain oversampling factor is 2 to extend the Doppler tolerance. We can determine from the simulation results which resampling ratio is the best choice.

The EVM and BER simulation results are shown in Tables 2 and 3. The length of the OCDM data block is the same for all cases with different various Doppler shift patterns. In the tables, cells with a yellow background highlight the best performance in each case. The average Doppler shift is zero for all various Doppler shift patterns because the length of the data block is unchanged, which also indicates that resampling is not required in the conventional method. The appropriate resampling ratio for the best performance (with the lowest EVM and BER) depends on the various Doppler shift pattern. If the pattern is known, the appropriate resampling ratio can be determined from the results in the tables. However, various Doppler shift patterns are generally complex and unpredictable in an actual UWAC.

The conventional method determines the resampling ratio by averaging the Doppler shift. However, in the case of time-varying Doppler shifts, this approach is inconsistent with the most appropriate resampling ratio. We adopt another method to detect the Doppler variation within the data frame. A single-frequency continuous wave (CW) can be inserted into the OCDM data frame to detect the short-term Doppler shifts. The CW-assisted Doppler shift estimation implementation is shown in Fig. 8(a). The CW signal (which can be expressed as $\sin(2\pi f_{CW}t)$) and the OCDM signal are superimposed and sent out. The frequency spacing between

TABLE 3. BER results for various doppler shift patterns and resampling ratios.

Doppler shift patterns			Resampling ratios				
A	B	C	$1/(1-\Delta)$	$1/(1-\frac{\Delta}{2})$	1	$1/(1+\frac{\Delta}{2})$	$1/(1+\Delta)$
1	Δ	0	$-\Delta$	0.06	0.002	0.002	0.02	0.1
2	Δ	$-\Delta$	0	0.2	0.05	0.002	0	0.03
3	0	Δ	$-\Delta$	0.3	0.08	0	0	0.01
4	0	$-\Delta$	Δ	0.3	0.1	0.02	0.008	0.05
5	$-\Delta$	Δ	0	0.4	0.3	0.1	0.02	0
6	$-\Delta$	0	Δ	0.3	0.2	0.03	0	0

TABLE 4. Statistical results of short-term doppler shifts.

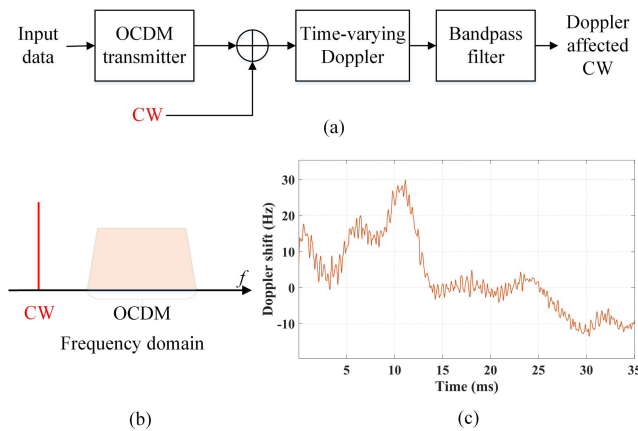| Doppler shift patterns			Estimated Doppler shift (Hz)			
A	B	C	Ave.	Std.	Max.	Min.
1	Δ	0	$-\Delta$	1.8	10.5	32.4	−15.7
2	Δ	$-\Delta$	0	4.9	12.5	44.1	−15.9
3	0	Δ	$-\Delta$	2.9	9.9	29.8	−15.4
4	0	$-\Delta$	Δ	3.3	13.1	49.6	−15.9
5	$-\Delta$	Δ	0	7	12.9	48.9	−20.7
6	$-\Delta$	0	Δ	4.4	10.2	43	−20.7

FIGURE 8. Implementation of CW-assisted time-varying doppler estimation. (a) the CW-assisted implementation process, (b) frequency spacing between CW and OCDM and (c) the short-term Doppler shifts.

FIGURE 9. Comparison of resampling techniques. (a) Single resampling and (b) multiplex resampling.

CW and OCDM is required. The time-varying Doppler-affected CW can be extracted by a bandpass filter, and then the short-term Doppler shifts can be measured by detecting the phase offsets in IQ demodulation, as shown in Fig. 8(c).

The statistical results based on CW-assisted Doppler shift estimation are summarized in Table 4, where the frequency of CW is 25 kHz. When carefully examining the statistical results of Doppler estimation (mean, standard deviation, maximum and minimum values) in Table 4, the standard deviation provides valuable information. It can be seen that the standard deviation values are similar to the Doppler variation of 10 Hz (i.de., ±1.2 km/h fluctuation range of the moving speed set in Fig. 7). The non-zero statistical mean is caused by the sudden change in Doppler shifts in the simulation. The valuable information (statistics) provided by Doppler estimation grasps more time-varying Doppler situations.

As mentioned above, even for a simple various Doppler shift pattern with only three parts, it is difficult to find the optimal resampling ratio if the pattern is unknown. For the actual UWAC, time-varying Doppler shifts caused by the irregular motion of the transmitter or receiver should be assumed to be almost unknown. In this paper, we consider using the statistical information in the short-time Doppler shifts and propose a multiplex resampling technique, i.de., extending the resampling range by the measured Doppler dispersion.

We compare the single resampling with the multiplex resampling in Fig. 9. The resampling ratio is determined based on the Doppler mean in single resampling. As long as the Doppler shift is constant within a data frame, single resampling can provide adequate performance for Doppler compensation. However, single resampling cannot cope with the case of time-varying Doppler shifts, especially when the Doppler pattern is unknown. The multiplex resampling extends the resampling range by using both the Doppler mean and standard deviation. An exhaustive search is performed in multiplex resampling to check the output of all extended resampling branches to search for the best resampling ratio.

III. DOPPLER-RESISTANT OCDM SYSTEM MODEL
A. EXPERIMENTAL AND SIMULATION MODELS
In this paper, the performance of the OCDM system with multiplex resampling is verified by experiment and simulation. The measured underwater acoustic channel is derived from a mobile UWAC experiment at the Qiandao Lake experimental field in Zhejiang, China. The simulated channel is generated using the stochastic mode of the channel simulator based on a given scattering function [22], and
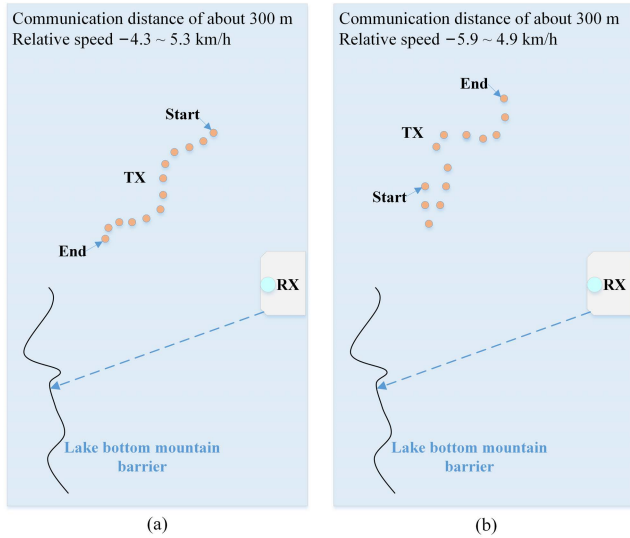
FIGURE 10. Relative position and movement trajectory of transmitter and receiver. (a) Actual motion in the Qiandao Lake experiment and (b) the assumed motion in the simulation.

time-varying Doppler shifts are added to the simulated channel to further verify the superiority of multiplex resampling.

We conducted a mobile UWAC experiment at the Qiandao Lake experimental field. The transmitter (TX) and receiver (RX) positions are plotted in Fig. 10. The depth of the lake at the experimental site is approximately 10 m, and the placement depth of the receiving transducer is approximately 3 m. The transmitting transducer is deployed at a depth of approximately 2 m as the boat moves, and the curve of the boat moves as shown in Fig. 10(a). The average boat speed is approximately 3.7 km/h (2 knots), and the relative Doppler speed between the TX and RX is not the same as the boat speed because the direction of the ship does not coincide with the direction of sound propagation. The Qiandao Lake experimental field is dominated by the muddy bottom. Note that the lake bottom topography is complex and that there is a mountain range under the lake at approximately 2.5 km from the experimental platform, which makes the communication signal-to-noise ratio (SNR) sharply drop and adversely affects the communication. Therefore, we kept the TX away from the underwater mountain range to avoid its influence.

Fig. 11 shows a measured normalized channel impulse response (CIR) for Qiandao Lake acoustic channel in Fig. 10(a). It can be seen that there is severe multipath interference with a long delay spread, and a relatively energetic multipath can be observed around 40 ms, which are generated by reflections from the water surface and lake bottom near RX. The intensity of the main path of acoustic propagation is significantly higher.

The duration of the original probe signal used to measure the underwater acoustic CIR is limited due to the experimental conditions (test duration, test environment, etc.). To further verify the effectiveness of multiplex resampling, we selected
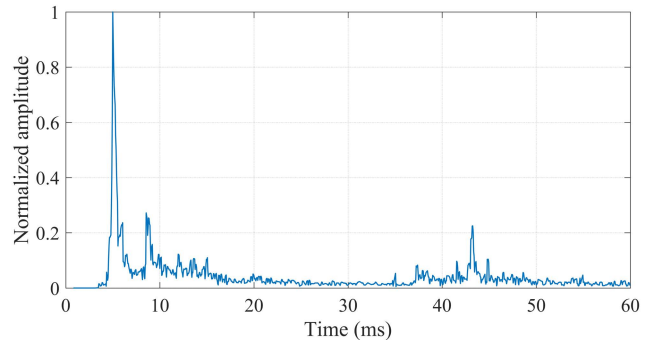

FIGURE 11. Normalized CIR for Qiandao Lake acoustic channel.

the stochastic replay simulator [23] to generate channel simulation data based on the measured channel in Fig. 11. The wide-sense stationary uncorrelated scattering (WSSUS) assumption is violated for the measured channel due to the movement of the transmitter. We can remove time-variable Doppler shifts around the mean by an iterative procedure, which is equivalent to a time-variable resampling factor in (13) applied to the recorded probe signal prior to delivery of the CIR $h(\tau, n)$ to the channel simulator [22].

$$R(t) = 1 - \frac{v_1}{c} + \frac{1}{2\pi f_c} \frac{d\theta(\tau_k, n)}{dt} \tag{13}$$

where v_1 is the average velocity of transmitter movement, c is the nominal sound speed, and $\theta(\tau, n)$ is the unwrapped phase of $h(\tau, n)$.

After iterative processing, the pre-set time-varying Doppler shifts can be added to the simulated channel with the true Doppler spectrum. The simulation assumes that the moving trajectory of TX is shown in Fig. 10(b) and that the average boat speed is set to 5.6 km/h (3 knots), and the pre-set time-varying Doppler shifts can be calculated according to the speed and moving trajectory. In this way, we can generate an arbitrary number of channel realizations.

B. DOPPLER-RESISTANT OCDM SCHEME

This section introduces the transmission and reception scheme in the Doppler-resistant OCDM communication system. The frame structure, modulation and demodulation of OCDM adopt the same scheme as previous work [2]. This scheme is compatible with the OFDM and only has IDFT and DFT operation processes at the transmitter or receiver.

As shown in Fig. 12(a), The IDFnT in OCDM modulation can be replaced by IDFT and two phase multiplications Θ_1^* and Θ_2^*, where Θ_1 and Θ_2 are diagonal matrices whose diagonal entries are $\Theta_1(m)$ and $\Theta_2(n)$, respectively. $\Theta_1(m)$ and $\Theta_2(n)$ can be expressed as:

$$\Theta_1(m) = e^{-j\frac{\pi}{4}} \times \begin{cases} e^{j\frac{\pi}{N}m^2} & N \equiv 0 \pmod 2 \\ e^{j\frac{\pi}{4N}} e^{j\frac{\pi}{N}(m^2+m)} & N \equiv 1 \pmod 2 \end{cases}$$

$$\Theta_2(n) = \begin{cases} e^{j\frac{\pi}{N}n^2} & N \equiv 0 \pmod 2 \\ e^{j\frac{\pi}{N}(n^2-n)} & N \equiv 1 \pmod 2 \end{cases} \tag{14}$$
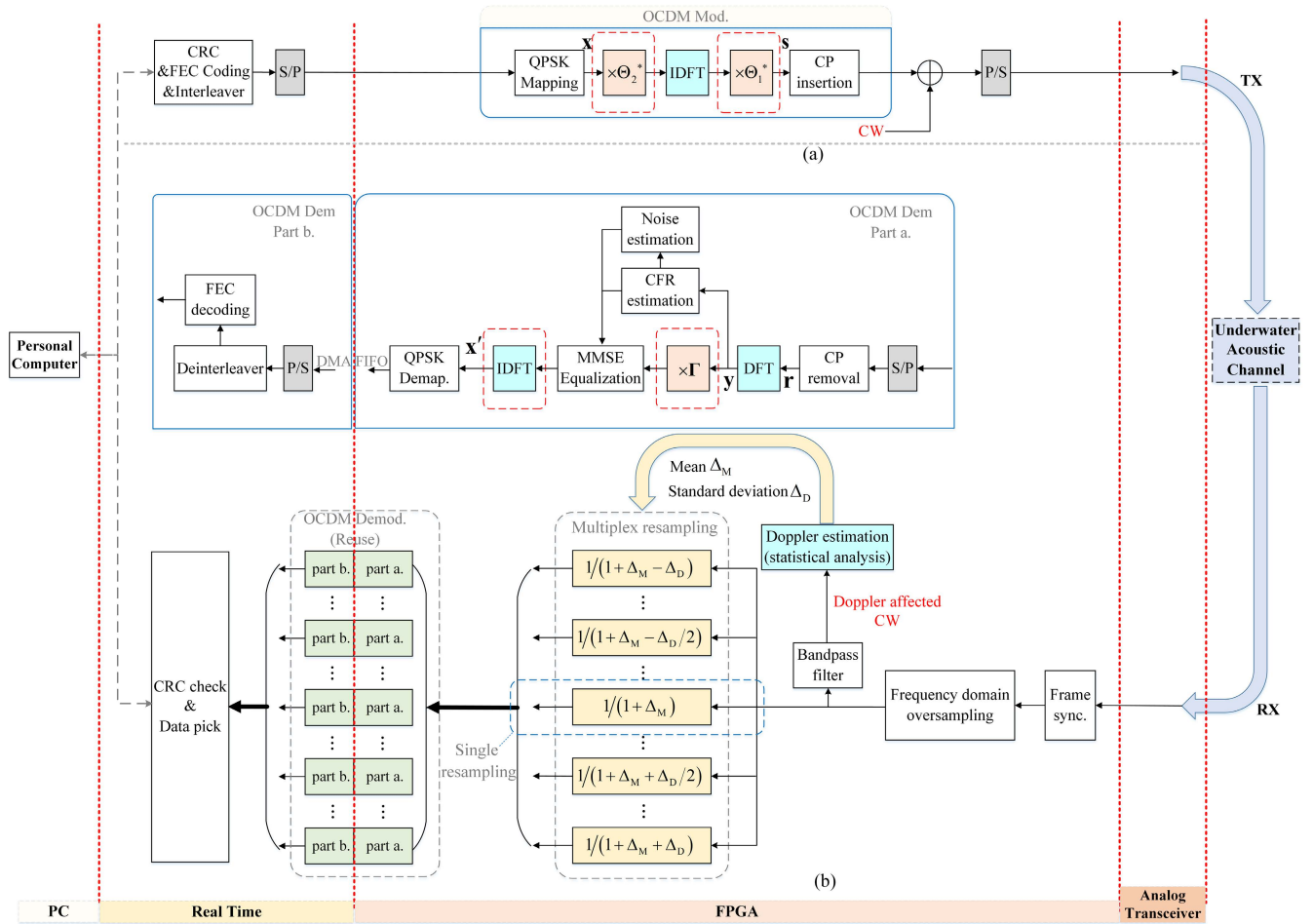
FIGURE 12. Schematic diagram of the Doppler-resistant OCDM system. (a) Transmitter and (b) receiver.

The receiver scheme of the Doppler-resistant OCDM system is shown in Fig. 12(b). The OCDM demodulation part adopts a single-tap frequency domain equalization (FDE) for the demodulation structure in [5]. The data block to be demodulated is $\mathbf{r}$, and DFT processing for $\mathbf{r}$ can obtain $\mathbf{y}$ before FDE. $\mathbf{y}$ can be expressed as:

$$\mathbf{y} = \mathbf{Fr} = \mathbf{\Gamma}^H \mathbf{F} \mathbf{\Lambda} \mathbf{x} + \mathbf{w} \qquad (15)$$

where $\mathbf{F}$ is the Fourier matrix of size N, both $\mathbf{\Gamma}$ and $\mathbf{\Lambda}$ are diagonal matrices of size N, which can be expressed as:

$$\{\mathbf{\Gamma}\}_{k,k} = e^{-j\frac{\pi}{N}k^2}$$
$$\{\mathbf{\Lambda}\}_{k,k} = H_k \qquad (16)$$

In (15), $\mathbf{w}$ is the Gaussian noise component with a mean of 0, and the variances of $\mathbf{w}$ and $\mathbf{x}$ are σ_w^2 and σ_x^2, respectively. In (16), H_k is the channel frequency response (CFR) of the channel at the kth frequency bin.

Assume that the CFR is unchanged in one frame; after performing phase multiplication, CFR compensation and IDFT processing on $\mathbf{y}$, the symbol $\mathbf{x}'$ estimate can be obtained. This process can be expressed as:

$$\mathbf{x}' = \mathbf{F}^H \mathbf{G} \mathbf{\Gamma} \mathbf{y} \qquad (17)$$

where $\mathbf{G}$ is the diagonal equalization matrix under the minimum mean square error (MMSE) criterion, which is obtained by pilot estimation and can be expressed as:

$$\mathbf{G} = \mathbf{\Lambda}^H (\mathbf{\Lambda}^H \mathbf{\Lambda} + \frac{\sigma_w^2}{\sigma_x^2} \mathbf{I})^{-1} \qquad (18)$$

The addition of the multiplex resampling receiver is shown in Fig. 12. The CW and OCDM signal are superimposed on the data frame at the transmitter. Frequency spacing is required between the CW and OCDM signal, where the frequency of the CW is 25 kHz, and the OCDM signal has a bandwidth of 30 kHz to 60 kHz. The CW is separated by a bandpass filter at the receiver, and the parallel Doppler estimation branch calculates the Doppler mean Δ_M and standard deviation Δ_D based on the measured short-term Doppler shifts. According to Δ_M and Δ_D, the resampling range is extended from $1/(1 + \Delta_M - \Delta_D)$ to $1/(1 + \Delta_M)$ to $1/(1 + \Delta_M + \Delta_D)$.

The Doppler-resistant OCDM receiver adopts multiplex resampling branches to resample and demodulate the received signal, and different resampling ratios are utilized in each branch. As discussed in Section II.dC, the appropriate resampling ratio depends on the various Doppler shift

TABLE 5. Examples of resampling ratios and number of resampling branches.

Doppler std. $\Delta_{\mathrm{D}} f_C$ (Hz)	Resampling range (10000:m)	Number of branches(N_{B})
5	9999, 10000, 10001	3
10	9998, 9999, 10000, 10001,10002	5
20	9996, 9997,9998, … ,10002, 10003, 10004	9

TABLE 6. Parameters settings for the experiment and simulation.

Symbol	Signification	Setting
B	Bandwidth for baseband signal	30 kHz
f_s	Sampling frequency	200 kHz
f_c	Center frequency	45 kHz
N	Number of subcarriers	1024
N_d	Number of data blocks per frame	4
T_{CP}	Cyclic prefix time	8.5 ms
T_G	Guard interval time after preamble sequence	256 ms
	Modulation	QPSK-OCDM
M	Constellation order	4
	FEC	Convolutional coding & Viterbi decoding
R_C	FEC rate	1/2
R_{CP}	Cyclic prefix ratio	1/4
N_B	Number of resampling branches	Dynamic adjustment (≤ 11)
α	Frequency domain oversampling factor	2

pattern. For unknown Doppler patterns, it will be challenging to obtain an appropriate resampling ratio by evaluating the received signal before demodulation, so an exhaustive search is performed in our study to solve this problem. At the transmitter, cyclic redundancy check (CRC) codes are inserted into the original data before forward error correction (FEC) coding. At the receiver, each data block is subjected to OCDM demodulation under each resampling branch with a different resampling ratio. The demodulated data are subjected to a CRC check and data pick to obtain the final information data, which corresponds to selecting the appropriate resampling branch without errors. If all resampling branches have data errors, the final data are generated by merging all decoded data in bit level. The added CRC overhead is typically small when using 16 bits (CRC-16).

The receiver's processing with multiplex resampling is shown in Fig. 12(b), where the single resampling is indicated with dashed lines, and the resampling ratio is $1/(1 + \Delta_{\mathrm{M}})$. The performance comparison of single resampling and multiplex resampling in UWAC is discussed in Section IV.

The relationship between the resampling range and the number of resampling branches in multiplex resampling is illustrated in Table 5, which shows examples of the resampling ratio and the number of resampling branches N_{B}. The resampling ratio can be expressed in the integer ratio form as follows:

$$\frac{1}{1 + \Delta_{\mathrm{M}} + \Delta_{\mathrm{D}}} = \frac{R}{R + \Delta'_{\mathrm{M}} + \Delta'_{\mathrm{D}}} \quad (19)$$

In (19), R is related to the resampling resolution mentioned in Section II.dB. When we set R to 10000 and Δ'_{M} to 0, the resampling ratio is 10000:10000 $+\Delta'_{\mathrm{D}}$ (integer ratio form). Note that the value of R depends on the Doppler tolerance and that the number of resampling branches can be set according to the Doppler measurements in Section II.dB. For a Doppler standard deviation of 5 Hz (where the mean is zero), the multiplex resampling employs three branches with resampling ratios of 10000:9999, 10000:10000, and 10000:10001. It follows that a trade-off between communication performance and computational complexity can be made in the multiplex resampling by the Doppler tolerance.

According to the UWAC experimental results, the number of resampling branches can generally be set to $N_{\mathrm{B}} = 11$. To further reduce the amount of computation, the number of branches can be dynamically adjusted in the experiment (we

refer to it as dynamic resampling branches). The process of dynamic resampling branches is presented as follows:

(a) Synchronize the received signal and extract the data frame
(b) Extract the CW signal through a bandpass filter and calculate Δ_{M} and Δ_{D}
(c) Determine the number of branches N_{B} according to Δ_{D}

Since the resampling ratio is adjusted in units of 1/10000 in the above example, the received signal for resampling should contain at least 10,000 samples. For the dynamic resampling branches, the Doppler standard deviation needs to be calculated for each frame, with a computational complexity of O(3N), which is much smaller than the computational complexity O($20N^2$) caused by the resampling (where N denotes the number of samples per frame). When the statistics of Doppler shift vary with the index of frames, the computational complexity can be reduced by dynamic resampling branches for each frame.

IV. SYSTEM EXPERIMENT AND SIMULATION RESULTS
A. SYSTEM PARAMETERS
In this section, the Doppler-resistant OCDM system is verified by experiment and simulation. Table 6 lists the parameter settings for the experiment and simulation. Since the experimental underwater acoustic channel is a doubly spread communication channel (Doppler spread and delay spread), the FEC rate is set to 1/2, and the communication rate is approximately 3.2 kbps.

B. RESULTS AND DISCUSSION
The Qiandao Lake experiment and simulation based on the stochastic replay channel correspond to the variations in SNR and relative Doppler velocity shown in Figs. 13 and 14,
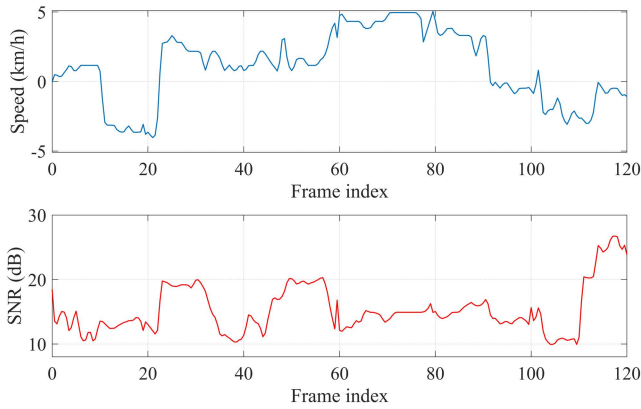
FIGURE 13. SNR and relative Doppler velocity in the Qiandao Lake experiment.
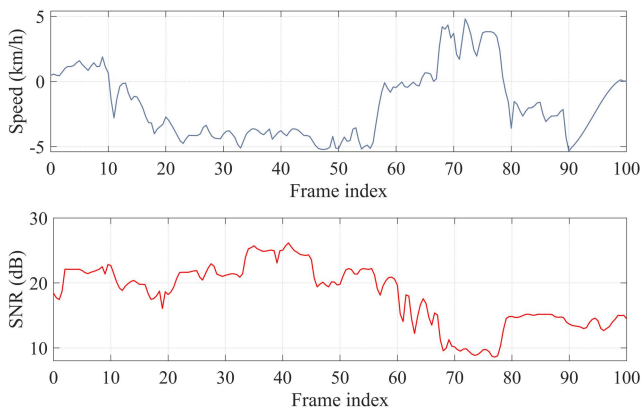

FIGURE 14. SNR and relative Doppler velocity in channel simulation.

respectively. The horizontal axes in the figures represent the data frame's index, and the Doppler variation can be observed throughout the communication process. Since the transmitter moves along the curve with the boat, the relative Doppler velocity changes with positive and negative values. The SNR also unevenly fluctuates, which may be caused by the wave disturbance and noise formed by the boat's propeller.

The BER performance and the number of resampling branches (N_B) of the Doppler-resistant OCDM system in the Qiandao Lake experiment are summarized in Fig. 15, while the BER performance and number of resampling branches based on channel simulation are summarized in Fig. 16. In both result plots, we use the BER results with no resampling as a benchmark for comparing the system performance with single resampling and multiplex resampling. For ease of viewing, the results with a BER of 0 are plotted on the performance line with BER = 10^{-4} on the vertical axis. As shown in Figs. 15 and 16, no resampling can significantly degrade the communication performance in the presence of time-varying Doppler shifts, with a BER of approximately 0.5 for most frames. Single resampling improves the communication performance and reduces the BER in many data frames, but some data frames still have errors (BER of approximately 0.5). Multiplex resampling
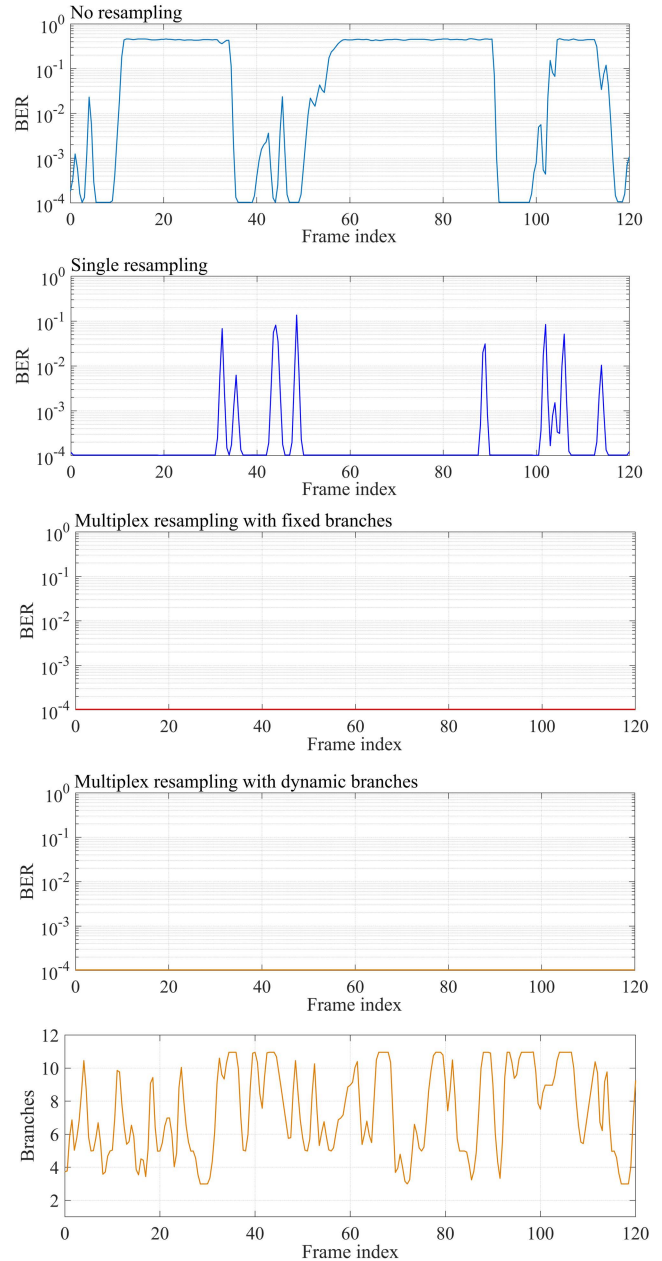

FIGURE 15. BER performance and the number of resampling branches in the Qiandao Lake experiment.

achieves better BER performance than no resampling and single resampling, and multiplex resampling was employed to successfully demodulate all data frames in the Qiandao Lake experiment (Fig. 15). A comparison of the fixed and dynamic branches in multiplex resampling shows that their BER results are consistent for all data frames, i.de., they have the same BER performance. The variation in the number of branches in the dynamic branches reveals that the number of branches is dynamically adjusted during the communication process, enables a reduction in the computational complexity of the Doppler-resistant OCDM system without sacrificing the communication performance.
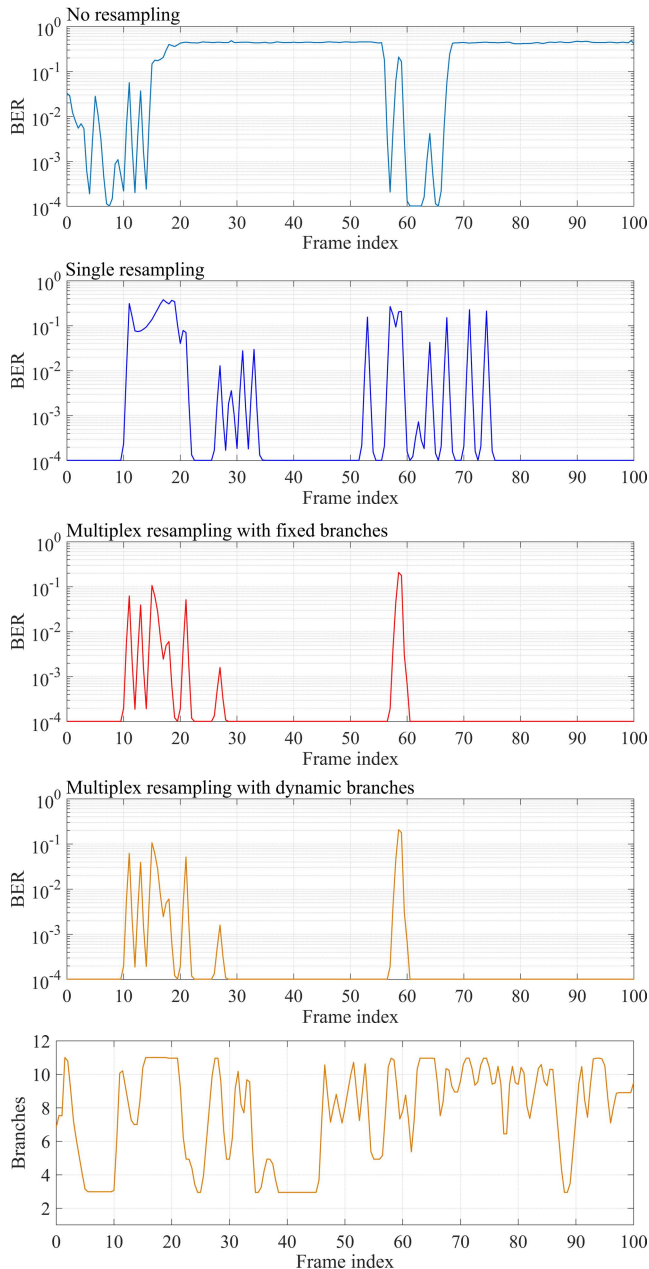
FIGURE 16. BER performance and the number of resampling branches based on channel simulation.

TABLE 7. Summary of experimental and simulation results.

	Single resampling		Multiplex resampling (fixed branches)		Multiplex resampling (dynamic branches)	
	Experiment	Simulation	Experiment	Simulation	Experiment	Simulation
FER	0.096	0.24	0	0.1	0	0.1
Number of branches(N_B)	1	1	11	11	7.4	7.9
Computational cost saving					$1-7.4/11$ $\approx 32.7\%$	$1-7.9/11$ $\approx 28.2\%$

The time-varying Doppler shifts measured at the 33rd, 49th and 102nd frames in the Qiandao Lake experiment
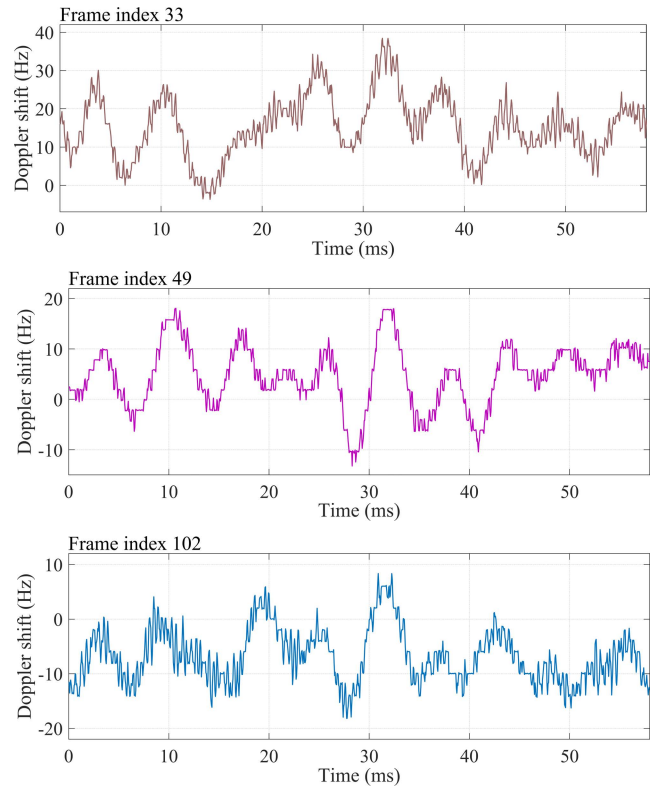

FIGURE 17. Time-varying Doppler shifts measured at the 33rd, 49th and 102nd frames in the Qiandao Lake experiment.

are shown in Fig. 17. The figure shows that the Doppler shift within the data frame fluctuates between positive and negative values as the transmitter moves. The 33rd, 49th and 102nd frames have BERs of 0.17, 0.45, and 0.37, respectively, in single resampling, while all the BERs in multiplex resampling are zero. This result shows that multiplex resampling can effectively improve the communication performance of OCDM in the presence of time-varying Doppler shifts.

The results of the Qiandao Lake experiment and simulation are summarized in Table 7, and the frame error ratio (FER) serves as the performance index. The single resampling achieved an FER of 0.096 and 0.24 in the experiment and simulation, respectively, while multiple resampling achieved an FER of 0 and 0.10. Multiplex resampling with dynamic branches can reduce the computational cost by 30% compared with fixed branches.

V. CONCLUSION

This paper proposes a new OCDM system with multiplex resampling for handling time-varying Doppler shifts in mobile UWAC. The OCDM is based on the Fresnel transform, which modulates the symbol by a set of orthogonal chirp signals. The effect of time-varying Doppler shifts on the performance of OCDM is investigated through a simplified various Doppler shift model. It is shown that the measured Doppler dispersion can provide adequate information to

grasp the time-varying Doppler situations. This paper further proposes an improved multiplex resampling, which extends the resampling range based on the measured Doppler standard deviation and thus reduces BER in mobile UWAC. We detail the implementation and parameter selection of the Doppler-resistant OCDM and compare the performance of multiplex resampling and single resampling by experiment in Qiandao Lake and by simulation. The BER and FER results verify the feasibility of multiplex resampling, and the Doppler-resistant OCDM has great application value in mobile UWAC. Compared with fixed branches, the application of the dynamic branches in multiplex resampling reduces the computational complexity and saves the computational cost by approximately 30%. In future work, we will consider further reducing the computational complexity by efficient channel estimation (e.dg., compressing sensing technique) and implementing the Doppler-resistant OCDM in an FPGA platform (NI CompactRIO) with a parallel mechanism.

REFERENCES

[1] A. Song, M. Stojanovic, and M. Chitre, "Editorial underwater acoustic communications: Where we stand and what is next?" *IEEE J. Ocean. Eng.*, vol. 44, no. 1, pp. 1–6, Jan. 2019.

[2] P. Zhu, X. Xu, X. Tu, Y. Chen, and Y. Tao, "Anti-multipath orthogonal chirp division multiplexing for underwater acoustic communication," *IEEE Access*, vol. 8, pp. 13305–13314, 2020.

[3] C. Baldone, G. E. Galioto, D. Croce, I. Tinnirello, and C. Petrioli, "Doppler estimation and correction for Janus underwater communications," in *Proc. IEEE Global Commun. Conf. (GLOBECOM)*, Taipei, Taiwan, Dec. 2020, pp. 1–6.

[4] K. B. Yoo and G. F. Edelmann, "Low complexity multipath and Doppler compensation for direct-sequence spread spectrum signals in underwater acoustic communication," *Appl. Acoust.*, vol. 180, Sep. 2021, Art. no. 108094.

[5] X. Ouyang and J. Zhao, "Orthogonal chirp division multiplexing for coherent optical fiber communications," *J. Lightw. Technol.*, vol. 34, no. 18, pp. 4376–4386, Sep. 15, 2016.

[6] M. Deguchi, Y. Kida, and T. Shimura, "Suppression of effects of Doppler shifts of multipath signals in underwater acoustic communication," *Acoust. Sci. Technol.*, vol. 43, no. 1, pp. 10–21, 2022.

[7] Y. Tabata, T. Ebihara, H. Ogasawara, K. Mizutani, and N. Wakatsuki, "Mobile underwater acoustic communication with orthogonal signal division multiplexing under inter-carrier interference larger than a guardband," *Jpn. J. Appl. Phys.*, vol. 60, no. 10, Oct. 2021, Art. no. 107003.

[8] X. Ma, T. Wang, L. Li, W. Raza, and Z. Wu, "Doppler compensation of orthogonal frequency division multiplexing for ocean intelligent multimodal information technology," *Mobile Netw. Appl.*, vol. 25, no. 6, pp. 2351–2358, Dec. 2020.

[9] B. S. Sharif, J. Neasham, O. R. Hinton, and A. E. Adams, "A computationally efficient Doppler compensation system for underwater acoustic communications," *IEEE J. Ocean. Eng.*, vol. 25, no. 1, pp. 52–61, Jan. 2000.

[10] B. Li, S. Zhou, M. Stojanovic, L. Freitag, and P. Willett, "Multicarrier communication over underwater acoustic channels with nonuniform Doppler shifts," *IEEE J. Ocean. Eng.*, vol. 33, no. 2, pp. 198–209, Apr. 2008.

[11] S. Beygi and U. Mitra, "Optimal Bayesian resampling for OFDM signaling over multi-scale multi-lag channels," *IEEE Signal Process. Lett.*, vol. 20, no. 11, pp. 1118–1121, Nov. 2013.

[12] K. Tu, T. M. Duman, M. Stojanovic, and J. G. Proakis, "Multiple-resampling receiver design for OFDM over Doppler-distorted underwater acoustic channels," *IEEE J. Ocean. Eng.*, vol. 38, no. 2, pp. 333–346, Apr. 2013.

[13] Z. Wang, S. Zhou, G. B. Giannakis, C. R. Berger, and J. Huang, "Frequency-domain oversampling for zero-padded OFDM in underwater acoustic communications," *IEEE J. Ocean. Eng.*, vol. 37, no. 1, pp. 14–24, Jan. 2012.

[14] T. Ebihara and G. Leus, "Doppler-resilient orthogonal signal-division multiplexing for underwater acoustic communication," *IEEE J. Ocean. Eng.*, vol. 41, no. 2, pp. 408–427, Apr. 2016.

[15] A. E. Abdelkareem, B. S. Sharif, C. C. Tsimenidis, and J. A. Neasham, "Compensation of linear multiscale Doppler for OFDM-based underwater acoustic communication systems," *J. Electr. Comput. Eng.*, vol. 2012, pp. 1–16, May 2012.

[16] T. MinhHai, S. Rie, T. Suzuki, and T. Wada, "An acoustic OFDM system with symbol-by-symbol Doppler compensation for underwater communication," *Sci. World J.*, vol. 2016, pp. 1–11, Feb. 2016.

[17] L. Wan, H. Jia, F. Zhou, M. Muzzammil, T. Li, and Y. Huang, "Fine Doppler scale estimations for an underwater acoustic CP-OFDM system," *Signal Process.*, vol. 170, May 2020, Art. no. 107439.

[18] L. Ma, H. Jia, S. Liu, and I. U. Khan, "Low-complexity Doppler compensation algorithm for underwater acoustic OFDM systems with nonuniform Doppler shifts," *IEEE Commun. Lett.*, vol. 24, no. 9, pp. 2051–2054, Sep. 2020.

[19] X. Ouyang, O. A. Dobre, Y. L. Guan, and J. Zhao, "Chirp spread spectrum toward the Nyquist signaling rate—Orthogonality condition and applications," *IEEE Signal Process. Lett.*, vol. 24, no. 10, pp. 1488–1492, Oct. 2017.

[20] H. F. Talbot, "LXXVI. Facts relating to optical science., no. IV," *London, Edinburgh, Dublin Phil. Mag. J. Sci.*, vol. 9, no. 56, pp. 401–407, Dec. 1836.

[21] C.-H. Hwang, K.-M. Kim, S.-Y. Chun, and S.-K. Lee, "Doppler estimation based on frequency average and remodulation for underwater acoustic communication," *Int. J. Distrib. Sensor Netw.*, vol. 11, no. 11, Nov. 2015, Art. no. 746919.

[22] R. Otnes, P. A. van Walree, and T. Jenserud, "Validation of replay-based underwater acoustic communication channel simulation," *IEEE J. Ocean. Eng.*, vol. 38, no. 4, pp. 689–700, Oct. 2013.

[23] P. A. V. Walree, T. Jenserud, and M. Smedsrud, "A discrete-time channel simulator driven by measured scattering functions," *IEEE J. Sel. Areas Commun.*, vol. 26, no. 9, pp. 1628–1637, Dec. 2008.

PEIBIN ZHU received the B.S. degree from the College of Ocean and Earth Science, Xiamen University, China, the M.S. degree from the College of Ocean and Earth Science, Xiamen University, in 2010, and the Ph.D. degree in underwater communications from the College of Ocean and Earth Science, Xiamen University, in 2020. From 2010 to 2016, he worked as a Research and Development Engineer at JX Instrument Company Ltd., Shanghai, responsible for the development of embedded test and measurement systems. He has been an Assistant Professor with the School of Ocean Information Engineering, Jimei University, since 2020. His research interests include underwater acoustic communication and networks, signal processing, virtual instrument, and data analysis.

GUANGSONG YANG received the Ph.D. degree from the School of Information Technology, Xiamen University. He was a Visiting Scholar at UC Davis, USA, from 2009 to 2010, and Griffith University, Australia, from 2017 to 2018. He is currently a Professor with the School of Information Engineering, Jimei University, Xiamen, China. His current research interests include underwater wireless sensor networks and security and intelligent information processing.

XIAOMEI XU received the M.S. degree in underwater acoustic telemetry and the Ph.D. degree in underwater communications from Xiamen University, China, in 1988 and 2002, respectively. From 1994 to 1995, she studied at Oregon State University, OR, USA. She is currently a Professor at the College of Ocean and Earth Science, Xiamen University. Her research interests include underwater communication, underwater acoustic telemetry, and underwater acoustic networks.

YOUGAN CHEN (Senior Member, IEEE) received the B.S. degree in communication engineering from Northwestern Polytechnical University (NPU), Xi'an, China, in 2007, and the Ph.D. degree in communication engineering from Xiamen University (XMU), Xiamen, China, in 2012.

He has visited the Department of Electrical and Computer Engineering, University of Connecticut (UCONN), Storrs, CT, USA, from November 2010 to November 2012. Since 2013, he has been with the College of Ocean and Earth Sciences, XMU, where he is currently an Associate Professor of applied marine physics and engineering. He has authored or coauthored more than 70 peer-reviewed journal articles/conference papers and holds more than 16 China patents. His research interests include the application of electrical and electronics engineering to the oceanic environment, with recent focus on cooperative communication and artificial intelligence for underwater acoustic channels.

Dr. Chen has served as the Secretary for IEEE ICSPCC 2017 and a TPC Member for IEEE ICSPCC 2019. He has received the Technological Invention Award of Fujian Province, China, in 2017. He has served as a Technical Reviewer for many journals and conferences, such as IEEE JOURNAL OF OCEANIC ENGINEERING, IEEE TRANSACTIONS ON COMMUNICATIONS, IEEE ACCESS, *Sensors*, *IET Communications*, and ACM WUWNet Conference. He has been serving as an Associate Editor for IEEE ACCESS, since 2019, and the Youth Editorial Board Member for the *Journal of Electronics and Information Technology*, since 2021.

WEN CHEN received the Ph.D. degree from Xiamen University, China, in 2011. Then, he became a Senior Engineer at ST Electronics (Satcom & Sensor Systems) Private Ltd., Singapore. In 2014, he led several projects about online structural health monitoring (SHM) of the optical ground wire in power transmission lines with distributed optical fiber sensor (OFS). Since 2018, he has been a Scientist II involved in distributed fiber sensor system development and application in I2R (A*STAR). He currently works at Jimei University, focusing on SHM and underwater acoustic signal processing.

· · ·